Numerical Simulation of the Response of an Unreinforced Brick-Masonry Cross Vault Subjected to Seismic Loading

César Chácara[1], Bartolomeo Pantò[2], Francesco Cannizzaro[3], Davide Rapicavoli[3], Ivo Caliò[3]

[1] Pontificia Universidad Católica del Perú, San Miguel Lima 15088, Lima, Perú. E-mail: c.chacara@pucp.pe

[2] Durham University South Road Durham, DH1 3LH, UK. E-mail: bartolomeo.panto@durham.ac.uk

[3] University of Catania, Department of Civil Engineering and Architecture, 95125 Catania, Italy. E-mail: francesco.cannizzaro@unict.it, davide.rapicavoli@unict.it, ivo.calio@unict.it

Abstract

This paper presents the numerical evaluation of the seismic response of a masonry cross vault using the Discrete Macro-Element Method (DMEM). The case study corresponded to a full-scale unstrengthened cross vault that was experimentally investigated within the scope of the **SERA Project – Seismic Response of Masonry Cross Vaults: Shaking table tests and numerical validations**. *The cross vault was subjected to repeated shaking table and dynamic identification tests until reaching significant damage. The numerical simulations involved the calibration of the Young's modulus of the masonry material aiming at reproducing the cross vault's experimental natural frequencies and mode shapes. The comparison of frequencies was carried out by estimating the difference between experimental and numerical results, whereas the correspondence between mode shapes was studied using the Modal Assurance Criterion. Subsequently, a sensitivity analysis was performed to identify the influence of nonlinear properties on the seismic response of the cross vault (displacement and acceleration time histories and failure mechanism). The accuracy of the numerical time histories was evaluated by estimating magnitude and phase discrepancies. The results aimed at demonstrating the applicability of the DMEM for assessing the seismic response of masonry cross vaults with an acceptable degree of accuracy and low computational cost.*

Keywords: HiStrA Software, Fiber calibration, Calibration procedure, Sensitivity analysis, Time history analysis.

1. Introduction

Masonry vaults constitute an essential structural component of architectural heritage. These curved elements enhance the structural performance of historical buildings in terms of

stiffness and capacity and provide cover or roof systems. Due to the mechanical properties of masonry, characterized by a strong inelastic behaviour, and the orthotropic nature associated with the arrangement of the units, these structural components generally present a weak performance when subjected to unexpected events such as differential settlements or earthquakes. The main causes of failure associated with this type of structure were reported in the work conducted by Theodossopoulos and Sinha (2008). For instance, lateral instability, originated by the outward spread of the supports, generates a central hinging line across the intrados of vaults and their detachment from adjacent walls. In addition, severe damage or even collapse of vaulted structures can be generated by in-plane distortions from surrounding elements caused by dynamic loading and the different stiffnesses along perpendicular directions. In this regard, the seismic response of these structures is also governed by the complex geometrical characteristics, the total mass, the presence of infill, and the constructive process. Lastly, another source of failure corresponds to design errors or inappropriate interventions. These aspects highlight the necessity for better understanding the structural performance of curved structural elements.

As reported in the literature review conducted by Bertolesi et al. (2019), the assessment of the response of curved structures, mainly ribbed or groin vaults, has been thoroughly investigated in the last two decades. Such investigations involved the application of different methodologies such as laboratory testing (Theodossopoulos et al., 2002; Foraboschi, 2004; De Matteis and Mazzolani, 2010; Krajewski and Hojdys, 2014; Fagone, Rotunno, and Bati, 2016; Milani et al., 2016; Rossi, Calderini, and Lagomarsino, 2016; Rossi et al., 2017; Torres et al., 2019; Bianchini et al., 2022), thrust-based approaches (Block and Ochsendorf, 2007; Angelillo, Babilio, and Fortunato, 2013; Rossi et al., 2017; De Lorenzis, Dimitri, and La Tegola, 2007; Fraternali, 2010; Coccia and Como, 2015), limit analysis (Block, Ciblac, and Ochsendorf, 2006; Milani, Milani, and Tralli, 2008; Milani, Milani, and

Tralli, 2009; Milani, 2015; Chiozzi, Milani, and Tralli, 2017; Gaetani et al., 2017), numerical simulations based on the Finite Element Method (FEM) (Creazza et al., 2002; Theodossopoulos et al., 2002; Theodossopoulos, Sinha, and Usmani, 2003; Milani, Simoni, and Tralli, 2014; Lengyel and Bagi, 2015; Milani et al., 2016; Angjeliu, Cardani, and Coronelli, 2019; Gaetani, Bianchini, and Lourenço, 2021; Alforno et al., 2022; Santini et al., 2022; Bianchini et al., 2023c), the Discrete Element Method (DEM) (McInerney and DeJong, 2014; Lengyel and Bagi, 2015; Lengyel, 2017; Foti, Vacca, and Facchini, 2018) and homogenization techniques (Milani and Tralli, 2012; Scacco, Milani, and Lourenço, 2020). Nevertheless, predicting this type of element's structural and seismic performance is still considered a complex and challenging task and presents some relevant limitations. For instance, experimental testing is costly and allows the assessment of fewer specimens. In this regard, vaulted structures experimentally investigated are usually subjected to vertical loading, neglecting the assessment of their lateral resistance.

On the other hand, numerical simulations, despite representing a more versatile methodology, usually require detailed models and significant computational burden and are primarily focused on specific structural typologies for academic purposes. It is worth noting that some numerical investigations related to historical buildings characterized by curved structures (Angjeliu et al., 2020; Saloustros, Pelà, and Roca, 2020) were recently conducted, considering the application of static loads. Nonetheless, this type of loading cannot correctly simulate the effects produced by earthquakes, such as material degradation and energy dissipation, which play a fundamental role in the seismic response of monumental masonry buildings.

Recent trends in modelling existing masonry buildings led to the introduction of numerous simplified approaches to studying conventional structures based on the assumption of box-type behaviour (Marques and Lourenço, 2011). Based on equivalent frame (Magenes

and Della Fontana, 1998; Kappos, Penelis, and Drakopoulos, 2002; Penna, Lagomarsino, and Galasco, 2014) or two-dimensional plane (D'Asdia and Viskovic, 1995; Casolo and Peña, 2007; Caliò, Marletta, and Pantò, 2012) configurations, such approaches have the great advantage of studying entire buildings in the nonlinear field with a reasonable computational effort, compatible with practical engineering. These formulations, characterized by reduced degrees of freedom (DOFs), focus the overall performance on the in-plane response of these structures, neglecting their interaction with out-of-plane mechanisms. Moreover, due to the adopted simplifications, most of these approaches are applied to structures with regular geometrical configurations. The latter constitutes a significant limitation of these techniques since they cannot be applied to curved structures. Adopting rigorous nonlinear Finite Element strategies for these monumental buildings is currently the only possibility for adequately assessing their seismic response.

This paper focuses on the application of an alternative modelling approach to assess the seismic performance of an unstrengthened brick masonry cross vault and to simulate its experimental response. This modelling approach follows the Discrete Macro-Element Method (DMEM), which was initially introduced by (Caliò, Marletta, and Pantò, 2012), further upgraded by [17], and implemented in the software HiStrA (Gruppo Sismica s.r.l., 2015). The reported numerical simulations refer to an experimental campaign that was carried out as part of the **SERA Project – Seismic Response of Masonry Cross Vaults: Shaking table tests and numerical validations,** and is briefly described in this paper. The experimental campaign comprised the mechanical characterization of fired brick masonry material through triplet-shear, uniaxial, and diagonal compression tests. In addition, it also considered the evaluation of an unstrengthened masonry cross vault by means of dynamic identification and shaking table tests. Initially, the numerical model was calibrated by fitting the experimental dynamic properties of the masonry cross vault under no damage conditions.

Subsequently, nonlinear dynamic analyses were carried out to simulate the observed seismic response of the masonry cross vault obtained from the shaking table tests. This stage of the study involved a sensitivity analysis regarding the material's nonlinear properties, namely tensile strength, cohesion, and tensile fracture energy. A comparison between experimental and numerical displacement time histories and failure mechanisms was carried out to evaluate the DMEM accuracy in simulating the dynamic nonlinear response of vaulted structures.

2. The Discrete Macro-Element Method strategy

The initial formulation of the Discrete Macro-Element Method (DMEM) was introduced by Caliò, Marletta, and Pantò (2012) for evaluating the in-plane seismic response of masonry structures. In the DMEM, a masonry wall is idealized by a set of two-dimensional panels composed of hinged rigid quadrilaterals whose connection is given by zero-thickness interface elements simulating the axial/flexural and sliding interactions between the connected panels. Additional model mechanisms accounting for the out-of-plane and torsional masonry responses were formulated and validated by introducing three-dimensional degrees of freedom to each macro-element, as reported by Pantò et al. (2017b).In this model, the proper simulation of the new mechanisms is given by zero-thickness interface elements. It is worth noting that the three-dimensional version of the DMEM has been effectively used in assessing unreinforced masonry, infilled reinforced-concrete (Caliò and Pantò, 2014), and monumental (Cannizzaro et al., 2018) construction typologies, and more recently, modelling fiber-reinforced polymers to retrofit masonry substrates (Cannizzaro et al., 2023; Pantò et al., 2017a). A comprehensive overview of the modelling strategy can be found in (Caddemi et al., 2017).

2.1. The mechanical model

For the plane DMEM formulation (see Figure 1a), the kinematic of a single panel is described by four degrees of freedom associated with the in-plane rigid body motion and the shear deformability. The 2D mechanical scheme allows for the description of the main in-plane mechanisms of masonry panels. Namely, the flexural mechanism is governed by a single row of links placed at the interface element, which are orthogonal to the edges of the panel (see Figure 1b), the in-plane shear sliding mechanism is simulated by a rigid-plastic link along the direction of the interface element (see Figure 1c), and the in-plane shear-diagonal is governed by one (or two) additional link located inside the panel (see Figure 1d).

Seven DOFs describe the upgraded mechanical scheme of the DMEM (see Figure 2a): six are related to the translational and rotational rigid body motion, and one is associated with the in-plane shear deformability. The additional mechanisms, namely torsional and out-of-plane responses, are simulated by new links introduced in an interface element (see Figure 2b). For instance, the transversal links are distributed in at least two rows along the interface element to simulate the biaxial bending mechanism. In contrast, two additional longitudinal links, placed along the thickness of the interface element, govern the out-of-plane shear deformability and torsion response of a portion of masonry, as described in detail in regard with the regular configuration element (Pantò et al., 2017b).

To accurately simulate the mechanisms involved with the three-dimensional panels, the elastic properties of the different sets of links are defined according to suitable calibration procedures. For instance, the stiffness associated with the shear-diagonal mechanisms is obtained by enforcing an equivalence between a finite portion of masonry considered as a continuum medium and the behaviour of the corresponding mechanical scheme when subjected to a pure shear strain field associated with the angular distortion Γ (see Figure 2c).

On the other hand, the flexural and shear-sliding mechanisms are calibrated following a fiber discretisation strategy given by the influence area of each link and describing the masonry at the macroscale as an equivalent continuum material. An example of the fiber approach selected for the calibration of the flexural and out-of-plane shear responses are depicted in Figure 2d and Figure 2e, respectively. Finally, the torsional response and the corresponding elastic stiffness estimation are calibrated by defining the proper distance between the two out-of-plane longitudinal links. Further details regarding the calibration procedure of the DMEM are reported in Cannizzaro et al. (2018) and Pantò et al. (2017b).

2.2. Nonlinear cyclic constitutive models

The nonlinear and cyclic behaviour of the DMEM is focused on the different sets of links that simulate the combined in-plane and out-of-plane mechanisms of masonry structures. For instance, the nonlinear behaviour of the diagonal link, which governs the in-plane shear diagonal mechanism, can be described either by the Mohr-Coulomb criterion or by the Turnsek and Cacovic (1971) yielding surface, accounting for the confinement forces applied to the panel (Figure 3a). In this case, the nonlinear behaviour of the shear-diagonal mechanism is defined mainly by a shear strength f_v and a friction coefficient μ_d. The cyclic response of this link is given by a Takeda hysteretic model (Takeda, Sozen, and Nielsen, 1970) in which initial or secant stiffnesses can rule the unloading cycles. On the other hand, the nonlinear behaviour of the transversal links is evaluated considering independent values of tensile f_t and compressive f_c strengths. Exponential softening curves can describe the tensile behaviour, whereas the compressive behaviour can adopt a parabolic curve (Figure 3b). The post-peak behaviour is ruled by fracture energy in tension (G_t) and compression (G_c). It is worth noting that the transversal links' cyclic behaviour can also be described by a Takeda hysteretic model (Takeda, Sozen, and Nielsen, 1970) or with different unloading

stiffness orientations for tensile and compressive behaviours governed by a coefficient β whose value ranges between 0 and 1. The β coefficient is equal to 0 when the unloading is oriented to the origin, and equal to 1 with an initial stiffness unloading. Finally, the nonlinearity of the links associated with the sliding behaviour is characterized by a plasticity Mohr-Coulomb yielding criterion given by its frictional phenomenon (Figure 3c) in which values of cohesion c and friction coefficient μ_s define the shear strength.

3. Mechanical characterization of masonry

The mechanical characterization of the masonry material was carried out at the National Laboratory of Civil Engineering - LNEC in Lisbon, Portugal. The laboratory testing involved the application of triplet shear tests as well as uniaxial and diagonal compression tests on fired brick masonry specimens. The laboratory testing also considered the mechanical characterization of masonry components such as solid-fired brick units and hydraulic lime mortar. In the case of the fired brick units, the laboratory testing involved the application of uniaxial compression tests (BS EN 772-1, 2011), whereas the mechanical characterization of the mortar considered three-point bending and uniaxial compression tests (EN 1015-11, 2006). Uniaxial compression tests were applied to six samples of units with approximate dimensions of 133 x 40 x 40 mm^3. From these tests, it was possible to estimate mean values (σ) and their corresponding coefficients of variation (COV) of properties such as Young's modulus and compressive strength. Two sets of dimensions were considered depending on the type of applied test involved in the mechanical characterization of mortar. The former was focused on three-point bending tests with dimensions of 160 x 40 x 40 mm^3. In contrast, the latter was related to the uniaxial compression tests in which the samples presented dimensions of 80 x 40 x 40 mm^3. From these tests, it was possible to estimate the mean values and COV of the main mechanical properties of mortar (Young's modulus

together with compressive and flexural strength). A summary of the mechanical properties of solid units and mortar samples is reported in Table 1. The following subsections present a more detailed description of the laboratory testing involved in the mechanical characterization of masonry as a composite material. Further details regarding the mechanical characterization can be found in the work conducted by Bianchini et al. (2023a).

3.1. Uniaxial compression tests

The mechanical characterization of masonry as a composite material involved the application of uniaxial compression tests following the recommendations given in (EN 1052-1, 1998). These tests were carried out on four wallets (W1, W2, W3, and W4) with average dimensions of 619 x 468 x 118 mm^3. These wallets were subjected to incremental uniform loading considering a displacement control setup with a constant velocity of 3 μm/s. As illustrated in Figure 4a, the measurements of displacements were carried out using six LVDTs on both faces of the masonry wallet. On each face, the instrumentation setup consisted of two vertical and one horizontal LVDTs whose initial distancing was approximately 330 mm and 360 mm, respectively. From the application of these tests, it was possible to determine the mechanical properties of the masonry material, such as Young's modulus and compressive strength. For instance, the compressive strength was estimated as the ratio between the maximum applied load and the cross-sectional area of the masonry wallets, presenting an average value of 9.10 MPa with a COV of 2%. Such reduced variability can also be observed in the stress-strain curves shown in Figure 4b, in which similar compressive strengths describe all four wallets. On the other hand, the Young's modulus was determined considering a stress value equal to one-third of the maximum stress and its corresponding average vertical strain of all four measurement positions. The Young's modulus presented an average value equal to 2223 MPa with a COV of 14%. In addition to

the Young's modulus, it was also possible to observe that the masonry wallets were also characterized by a slight variation in terms of deformation capacity in which the ultimate vertical strains ranged between 0.01 mm/mm and 0.016 mm/mm.

3.2. Diagonal compression tests

The characterization of the shear strength and shear modulus of the material involved the application of diagonal compression tests to two fired brick masonry wallets (W5 and W6) based on the recommendations reported in (ASTM E519/E519M – 10, 2010). These wallets, with average dimensions 980 x 1000 x 110 mm^3, were instrumented with a total of four LVDTs: two on each face (see Figure 5a). One transducer measured the vertical displacements on each face, and the other registered the horizontal ones. The specimens were diagonally placed on a testing machine, and a uniformly distributed load was applied through a steel shoe with a constant velocity of 5 µm/s up to collapse. From these tests, it was possible to estimate average values of shear strength and shear modulus equal to 0.44 MPa and 762 MPa, respectively. However, from the curve shown in Figure 5b, it was observed that significant differences in vertical and horizontal ultimate strains characterized the masonry wallets.

3.3. Triplet shear tests

The shear strength of mortar joints was evaluated through triplet shear tests according to the standard EN 1052-3:2002 (EN 1052-3, 2002). These tests were performed on twelve samples of three fired brick units with total approximate dimensions of 17.3 x 22.3 x 11.8 cm^3. As illustrated in Figure 6, the experimental setup consisted of applying a vertical uniform load at the middle brick with a constant velocity of 0.05 µm/s. The exterior bricks were subjected to pre-compressive loads equal to 0.2 MPa, 0.5 MPa, and

0.8 MPa to account for confinement effects. In addition, the measurement of vertical displacements was carried out using two LVDTs. From these tests, it was possible to determine the cohesion and the friction coefficient, which resulted in 0.031 MPa and 0.785, respectively.

4. Dynamic experimental testing

Within the scope of the **SERA Project – Seismic Response of Masonry Cross Vaults: Shaking table tests and numerical validations**, the dynamic response of an unstrengthened masonry cross vault was experimentally investigated at the LNEC in December 2020. The experimental campaign comprised the dynamic identification and shaking table tests to an unstrengthened brick-masonry cross vault to estimate its main modal properties and assess its seismic response. The full-scale masonry specimen was subjected to four shaking table tests considering increasing seismic intensities, namely 10%, 25%, 50%, and 75% of the 2009 L'Aquila earthquake. In addition, the first natural frequencies were measured via forced vibrations considering artificial accelerograms along the main horizontal directions. The Dynamic Identification Tests (DIT) were carried out at the end of each shaking table test to correlate the changes in the dynamic properties of the vault with the accumulated structural damage occurred during the different forced vibration tests. A summary of the sequence of dynamic identification and shaking table tests is reported in Table 2.

4.1. Unstrengthened cross vault

The cross vault was built using solid-fired brick units with average dimensions of 45 x 120 x 230 mm^3 and approximately 10 mm thick mortar joints. The arrangement of the units was carried out with bed joints aligned orthogonally to the 3.5-meter edges of the cross

vault. A non-structural masonry compound or infill was placed on each corner of the cross vault to restrain the masonry webs and account for additional weight. Furthermore, steel plates were placed in these non-structural compounds to provide additional rotational restrains at the four corners of the cross vault. Two sets of boundary conditions, denoted as fixed and moveable edges, were defined to ensure the occurrence of an in-plane shear mechanism. The former, applied to two corners, were supported by masonry piers that simulated the presence of walls and columns and were laterally restrained through steel profiles fixed to the base of the shaking table. The latter, applied to the remaining two corners, were located on steel supports connected to the shaking table through wheels, enabling the displacements along horizontal directions (X- and Y-axes) and the rotation around the vertical direction (Z-axis). Finally, the full-scale specimen included steel bars, which were used to connect the masonry piers to the steel supports to simulate the conditions and behaviour of actual vaulted structures. Plan and isometric views of the masonry cross vault and its corresponding boundary conditions are depicted in Figure 7a and Figure 7b, respectively.

4.2. Experimental setup

During the experimental campaign, several response parameters were measured using a wide range of sensors as part of the instrumentation setup. For instance, piezoelectric accelerometers (*ACC*) were placed in 17 points distributed along four edges, on each infill compound and top of the masonry cross vault, measuring overall 29 directions. It is worth noting that the accelerations recorded at the shaking table were also measured by introducing additional piezoelectric accelerometers. The displacements were measured using four optical cameras (*OC*): one placed at the top of the masonry cross vault and the remaining three along the moveable edge. The overall seismic performance of the cross vault was captured using

five video cameras (*VC*) whose positions were in front of each edge and on top of the masonry vault. Finally, load cells were also introduced as part of the instrumentation setup to register the history of axial forces at the steel rods. A scheme that illustrates some of the sensors used to record structural parameters and their corresponding position is shown in Figure 8.

4.3. Dynamic identification

The dynamic properties of the vault were experimentally identified at the end of the four shaking tests, corresponding to as many damage scenarios of the vault. The first dynamic identification test (DIT 0) was performed considering the undamaged condition of the prototype. The remaining three dynamic identification tests (DIT 1, DIT 2, and DIT 3) were performed after the shaking table tests with 25%, 50%, and 75% of the same seismic input, represented by 160-second artificial accelerograms applied along the two principal horizontal directions of the vault. The transducers used for registering the signals corresponded to piezoelectric accelerograms with a sensitivity of 100 mV/g and a dynamic range of ±50 g pk, whereas the sampling frequency was equal to 200 Hz. The signal processing was carried out using the Frequency Domain Decomposition method implemented in the ARTeMIS software (Structural Vibration Solution, 2015).

Based on the signal processing, it was possible to identify the three fundamental vibration modes of the vault for all the damage scenarios but the last one. In all tests, the first vibration mode resulted in a pure shear deformation mode, associated with a natural frequency of 6.15 Hz in the undamaged condition; such a value did not significantly change after applying the 10% and 25% seismic input. Nonetheless, approximately 4.2% and 9.4% reductions were identified in the third and fourth damage scenarios, respectively. The second vibration mode resulted in the horizontal displacement of the moveable edge and presented a

natural frequency of 11.62 Hz in the undamaged scenario and reduced to 11.38 Hz, 10.79, and 10.10 Hz in the case of DIT 1, DIT 2, and DIT 3, respectively. Finally, the third vibration mode is governed by the vertical displacements with maximum values at the centre of the vault and associated with a frequency of 19.39 Hz, which did not experience any significant variation in DIT 1 and DIT 2. It is worth noting that the third mode was not identified in the last damage scenario. The experimental mode shapes and frequencies are reported in Figure 9. More details can be found in (Bianchini et al., 2023b).

4.4. Shaking table test

These tests were carried out using the shaking table available at the LNEC laboratory, applying the 2009 L'Aquila earthquake record (see Figure 10), considering increasing amplification factors of 25% until the failure of the structure. The signal was subjected to a baseline correction and a bandpass filtering process. The loading direction corresponded to the Y-axis, aiming at guaranteeing the activation of the in-plane shear failure mechanism of the unstrengthened masonry cross vault.

The failure mechanism of the unstrengthened masonry cross vault occurred at the shaking table test with 75% of seismic input. The failure mechanism was characterized by cracking propagating along both diagonals of the vault, evidencing a shear mechanism in the *xy* plane. Furthermore, additional cracks orthogonal to the cross vault's edges were observed in most of the masonry webs. This damage pattern can be explained by the activation of plastic hinges along the span of the perimetral arches due to their nonlinear flexural response. Moreover, detachment between the masonry webs and the infill compounds was identified in the corners of the fixed edge. This behaviour is clearly caused by the fully restrained condition of those corners, which do not allow rotations around the vertical direction as required by the global shear deformation motion of the vault. A general scheme of the failure

mechanism of the unstrengthened masonry cross vault is illustrated in Figure 11a. The relative displacements along the Y-axis of the measured points were also assessed for the shaking table tests with 75% of seismic input. The horizontal displacement of the moveable edge presented maximum and minimum values ranging between 16 mm and 19 mm in the positive direction and around 13 mm in the negative direction (considering OC3 and OC4 in Figure 8). Those displacements resented a slightly reduced value when assessing the top of the masonry cross vault (+14 mm and 10.5 mm). The deformed configuration of the unstrengthened masonry cross vault is represented in Figure 11b.

5. Numerical simulations

The DMEM model of the unstrengthened masonry cross vault was developed employing the HiStrA software (Gruppo Sismica s.r.l., 2015) to simulate its response under earthquake excitations. The actual geometrical characteristics of the different components of the full-scale specimen were considered to increase the accuracy of the numerical simulations. In this sense, the masonry vault, infill compounds, masonry binder, and steel elements were modelled using 3D macro-model elements, whereas steel rods were incorporated using truss elements (see Figure 12a). To reproduce the actual boundary conditions of the experimental tests, full restraints were assigned to the two fixed vault supports, while vertical displacements were restrained to simulate the willed supports (with free translation along the X- and Y- axes), as illustrated in Figure 12b. It is worth noting that, considering the distribution of wheels below the steel masses, it was assumed that the rotation around the vertical axis was enabled. Based on the number of panels and the defined boundary conditions, the DMEM model of the unstrengthened masonry cross vault was described by 5542 DOFs.

The simplified hypothesis of isotropic masonry material was adopted for the analyses. The numerical simulations initially involved a calibration of the linear elastic mechanical properties to simulate the experimental natural frequencies and mode shapes. Subsequently, a sensitivity analysis of the nonlinear characteristics of the masonry material was carried out to assess their influence on the masonry cross vault's seismic response and reproduce the experimental results in terms of displacement and acceleration time histories and failure mechanism.

A thorough comparison between numerical and experimental displacement time histories was carried out since it constitutes a primary structural parameter for assessing the nonlinear response of the masonry cross vault. For this purpose, the percentage errors of the DMEM model in predicting the maximum and minimum response displacements (relative to the shaking table displacements) were computed for each measured point. Moreover, two additional criteria associated with relative magnitude ε_M and phase ε_P errors (Russell, 1997) were considered for assessing the accuracy of the numerical results. The error ε_M, given by Equation 1, measures the ratio between the orders of magnitude of the numerical $\mathbf{d}_1$ and experimental $\mathbf{d}_2$ time histories, which can be approximately expressed as 10^{ε_M}. The error ε_P is expressed in Equation 2 and measures the phase consistency of the two compared responses. This error parameter ranges from 0, indicating no phase error, and 1 when data is fully out-of-phase.

$$\varepsilon_M = \operatorname{sign}\left(\frac{\mathbf{d}_1\cdot\mathbf{d}_1-\mathbf{d}_2\cdot\mathbf{d}_2}{\sqrt{(\mathbf{d}_1\cdot\mathbf{d}_1)(\mathbf{d}_2\cdot\mathbf{d}_2)}}\right)\log_{10}\left(1+\left|\frac{\mathbf{d}_1\cdot\mathbf{d}_1-\mathbf{d}_2\cdot\mathbf{d}_2}{\sqrt{(\mathbf{d}_1\cdot\mathbf{d}_1)(\mathbf{d}_2\cdot\mathbf{d}_2)}}\right|\right) \quad \text{Equation 1}$$

$$\varepsilon_P = \frac{1}{\pi}\cos^{-1}\left(\frac{\mathbf{d}_1\cdot\mathbf{d}_2}{\sqrt{(\mathbf{d}_1\cdot\mathbf{d}_1)(\mathbf{d}_2\cdot\mathbf{d}_2)}}\right) \quad \text{Equation 2}$$

5.1. Numeric fitting of experimental dynamic properties

In this section, the model's accuracy in predicting the dynamic properties of the vaults is evaluated. For this purpose, parametric analyses were performed to evaluate the model sensitivity to the linear elastic mechanical properties of the masonry material (Young's and shear moduli). An assessment of their influence on the corresponding natural frequencies and mode shapes to evaluate the macroscale model parameters that provide the best fit of experimental results has been also performed. The accuracy of natural frequencies was evaluated through absolute errors between numerical and experimental results, whereas the mode shape resemblance was determined using the Modal Assurance Criterion (MAC) evaluated by considering the monitored points in the investigated directions. Such criterion evaluates the correspondence between experimental and numerical mode shapes, and it presents a value ranging between 0 and 1 in which the former relates to a lack of similarity and the latter indicates a perfect coincidence (Allemang, 1982). It is worth noting that the experimental results considered for the calibration procedure corresponded to the undamaged condition.

Initially, the initial elastic mechanical properties were defined according to the average values obtained from the laboratory tests, which resulted in 2,223 MPa and 762 MPa, respectively, for the masonry Young's and shear moduli, and 22.55 kN/m^3 for the specific weight. For the steel material, typical values of Young's modulus, Poisson's ratio, and specific weight were adopted in the analyses, presenting values of 210 GPa, 0.25, and 78.5 kN/m^3, respectively. From the numerical simulations conducted using these nominal values, the first dynamic property resulted in a pure shear vibration mode with a natural frequency of 7.30 Hz. The second and third numerical vibrations modes, associated with the frequencies 20.63 Hz and 20.84 Hz, respectively, were characterized by a rotation of the steel masses and

horizontal translational displacement along the X-direction. The fourth vibration mode, with a natural frequency of 23.64 Hz, corresponded to the masonry cross vault's vertical displacement with the steel masses' slight rotation. The first four vibration modes predicted by HiStrA and their corresponding frequencies are shown in Figure 13.

Comparing the results of the numerical model with the experimental findings, it can be observed that the first and fourth numerical modes corresponded to the first and third experimental ones, respectively. Nonetheless, the numerical model could not simulate the second experimental vibration mode. The comparison in terms of frequencies evidenced significant differences, approximately 19% and 22% in the case of the first and third experimental modes, respectively. On the other hand, a significantly low value of MAC equal to 0.47 was obtained when comparing the agreement between the third experimental and fourth numerical mode shapes. The results in terms of frequencies and MAC values are summarised in the first column of Table 3.

The high numerical natural frequency values may be associated with the simplified kinematics of the DMEM model, the formation of micro-cracks caused during the prototype's preparation, or the values determined in the mechanical masonry characterization, which may not fully represent those characterizing the vault prototype. Therefore, a sensitivity analysis of the masonry material's Young's and shear moduli was performed to improve the correspondence between experimental and numerical results. The nominal value of Young's modulus was subjected to five reduction factor RF that ranged between 0.9 to 0.5 with decreasing steps of 0.1, keeping constant the ratio between shear and Young's modules of 0.343. The results of parametric analyses are summarized in Table 3. It is possible to observe that the correspondence in terms of frequencies improved by reducing the masonry moduli, reaching the minimum global error when a value of 0.6 of the reduction factor. In this case, the maximum error resulted in less than 4%. Also, the MAC ratio increased, with the

minimum value, corresponding to the third mode increased from 0.47 to 0.74, which can be accepted as a satisfactory value, considering the level of uncertainties potentially affecting the non-homogeneous masonry material and boundary conditions with possible friction between the wheels and the shaking table. The first and fourth modes, associated with a pure shear response and the vertical displacement of the cross vault, are shown in Figure 14.

5.2. Nonlinear time history analyses

After the model calibration performed in Section 5.1, the DMEM model of the masonry cross vault was used to perform nonlinear dynamic analyses to investigate its seismic response and evaluate the accuracy of the proposed approach. The solution of the dynamic equation of motion involved the application of the Newmark method based on an average acceleration approach, whereas the energy dissipation due to mechanisms not explicitly included in the model mechanic nonlinearities was modelled considering a viscous Rayleigh damping model. For the latter, two vibration modes with approximately 70% and 85% of cumulative effective mass along the direction of analysis and an initial damping coefficient of 5% were considered for the analyses.

The nonlinearity focused on the masonry material's mechanical properties (compressive and tensile strengths and cohesion). An elastoplastic constitutive law described the masonry flexural response based on different values of fracture energies in tension and compression, considering parabolic and exponential post-peak softening behaviours in compression and tension, respectively. According to the results of material tests, a peak strength of 9.10 MPa and a ductility index of 1.6 mm were considered in compression. The tensile strength, experimentally evaluated by diagonal compression tests, was 0.44 MPa, while the fracture energy in tension was assumed 0.02 N/mm, as suggested by Milani, Simoni, and Tralli (2014). A Mohr-Coulomb elastoplastic yielding criterion was used to

simulate the shear-sliding mechanism occurring at mortar joints considering the friction coefficient obtained by experimental tests ($\mu_s = 0.785$). Material tests provided a significantly low cohesion value compared to the tensile strength. However, a value of cohesion $c = 1.5\ f_t$ was adopted in the analyses (Ghiassi and Milani, 2019). A summary of the initial nonlinear properties for the seismic assessment of the unstrengthened masonry cross vault is reported in Table 4. In the case of the steel elements, a linear elastic behaviour was considered for the seismic assessment of the masonry cross vault.

The numerical simulations have been performed by applying the main three seismic inputs involved during the experimental shaking table tests, namely 25%, 50%, and 75% of L'Aquila record. These seismic inputs, shown in Figure 15, corresponded to the history of acceleration registered at the base of the shaking table, which were further subjected to a baseline correction and filtering process. Aiming to account for the accumulation of damage, these seismic inputs were applied sequentially.

The comparison between experimental and numerical results was carried out in terms of histories of relative displacements along the Y-Y direction. In this regard, the response of points OC1, OC3 and OC4 (see Figure 8 in Section 4) of the experimental instrumentation setup was considered for comparison purposes. These results are shown in Figure 16, in which the numerical response is superimposed on experimental findings. It was possible to observe significant differences in maximum relative displacements, especially for 50% and 75% seismic inputs, where the numerical model predicted almost an elastic response of the vault. In contrast, the experiments evidenced significant damage causing significant residual displacements. Overall, the numerical model underestimated the peak values of relative lateral displacements of the vault, with increasing differences as the amplitude of the

seismic input increases. These results showed that the nonlinear mechanical properties, directly evaluated from the tests at the material level, need to be updated.

In this regard, it was necessary to assess the influence of nonlinear and model parameters of the DMEM model on the seismic response of the unstrengthened masonry cross vault to improve the correspondence between experimental and numerical results. This assessment involved a sensitivity analysis concerning the main mechanical properties such as tensile strength, cohesion, and tensile fracture energy and model parameters such as damping coefficient.

First, a reduced damping coefficient of 2% was adopted to perform the analysis under 25% of seismic input, leading to a better correspondence between experimental and numerical results in terms of peak-displacement values. Second, the adoption of lower values of tensile strength, cohesion, and tensile fracture energy strongly influenced the response of the DMEM in the case of 50% and 75% of seismic input. The sensitivity analysis showed that the correspondence between numerical and experimental results improved when considering a tensile strength of 0.05 MPa, a cohesion of 0.075 MPa, and a tensile fracture energy of 1 N/m. Based on these values, it was evidenced that there was a successful agreement between the experimental and numerical history of relative displacements of all three measured points when assessing the seismic response of the cross vault due to the application of 50% of seismic input. Comparing relative displacements obtained from applying the 75% of seismic input presented a reasonable agreement. In this case, it was observed that the DMEM model could simulate similar maximum and minimum relative displacements. However, it is worth noting that the numerical model could not accurately reproduce the residual displacement obtained experimentally. This result may be justified with the simplified constitutive models adopted in the simulations that do not account for the

material's progressive stiffness and cyclic strength degradation. Nonetheless, the results, which are shown in Figure 17, can still be considered acceptable.

The errors in the peak response (maximum and minimum displacement registered values) and the magnitude and phase errors, summarized in Table 5, were computed for each monitored point of the different seismic intensities. In the case of the maximum displacement, it was observed that the errors ranged between 1% and 37%, whereas in the minimum one, these values varied from 1% to 30%. This wide range of errors may not correctly assess the entire transient data since it considers only one point. In addition, these values may not consider other possible error factors, such as the residual displacement that the numerical model did not capture. In this regard, estimating the magnitude and phase errors may lead to a more representative comparison of the histories of displacements since they account for all the transient data. In the case of the 25% of seismic intensity, the results of OC4 were characterized by a low magnitude error, indicating a good agreement in the history of displacement. On the contrary, points OC1 and OC3 were described by a slightly higher error. The magnitude errors associated with the 50% of seismic intensity presented considerably low values, demonstrating the accuracy of the numerical results. It is worth noting that the negative sign indicates that the numerical results are higher in terms of magnitude in contrast to the experimental ones. Finally, 75% of seismic input results were also characterized by slightly higher values of magnitude error. This could also be noticed in Figure 17 since the numerical model could not reach the maximum displacements, specifically in points OC1 and OC3. Finally, the phase error ranged between 0.18 and 0.37, indicating that numerical and experimental displacement time histories are reasonably in phase.

The comparison between experimental and numerical results was also carried out in terms of acceleration time history. This comparison involved the same three points from the

experimental setup, in this case, denoted as ACC18, ACC16, and ACC2 (see Figure 8 in Section 4). As illustrated in Figure 18, it was observed that for a low-intensity seismic input, the correspondence between numerical and experimental results was in good agreement since similar acceleration amplitudes were obtained with the DMEM model. However, in the case of higher intensities (50% and 75% of seismic input), the DMEM model slightly overestimated acceleration amplitudes. This behaviour was most noticeable in the centre of the lateral arch (ACC16) and on top of the infill compound (ACC2).

5.3. Damage assessment

The numerical failure mechanism and the damage pattern obtained from applying the three seismic inputs were also evaluated to demonstrate the model's capability to predict the experimental damage pattern. In the case of 25% of seismic input, illustrated in Figure 19a, the numerical model did not evidence any damage concentration in terms of plastic strains. This result confirms what was already discussed, commenting on the comparisons in terms of displacement time histories at this input level, where the numerical model almost behaved in an elastic range. The response of the DMEM model associated with 50% of seismic input also involved damage along the diagonal which might be associated with a micro cracking that was not visible during the experimental tests. Nonetheless, in the case of 25% and 50% of intensity, it was noted that the detachment of the infill compound in the corners of the masonry cross vault. This behaviour was not observed in the numerical results. Finally, applying the seismic input with 75% of intensity involved the failure mechanism of the unstrengthened cross vault, mainly consisting of the total activation of plastic hinges along the masonry web and damage concentrated along the diagonal. In addition, it was possible to observe that damage concentrated between the masonry web and the infill compound at all four corners. The failure mechanism and damage concentration of the

DMEM model of the unstrengthened masonry cross vault due to the 75% intensity is illustrated in Figure 19c. Based on the latter results, it was evidenced that there was a reasonable agreement in terms of failure mechanisms between experimental and numerical results.

6. Final considerations

This paper reported the seismic response simulation of an unstrengthened masonry cross vault using an innovative numerical tool based on the Discrete Macro-Element Method. This numerical investigation was carried out in the scope of the **SERA Project – Seismic Response of Masonry Cross Vaults: Shaking table tests and numerical validation**. The project involved the application of shaking table tests to a full-scale masonry cross vault and the mechanical characterization of its constituent material.

In this investigation, the numerical model was initially calibrated to simulate the dynamic properties of the masonry cross vault obtained from an experimental dynamic identification. The calibration procedure demonstrated that the value of Young's modulus from the material characterization did not correspond to the actual properties of the masonry cross vault. It was evidenced that almost half of the value obtained experimentally allowed a proper simulation in terms of natural frequencies and mode shapes. This substantial difference may be associated with the lack of pre-compression stresses or confinement conditions that described the status of the masonry cross vault. A similar trend regarding the nonlinear properties was evidenced when comparing the histories of relative displacements obtained from the shaking tables tests. More in detail, the tensile strength value obtained from the mechanical characterization led to a significant underestimation of the experimentally observed response. Therefore, it was necessary to reduce its initial value to almost 10% to reproduce the experimental results. The numerical analyses made it possible to determine the

influence of other mechanical and model properties, such as tensile fracture energy and damping coefficient. Overall, the numerical model could properly simulate the seismic response of an unstrengthened masonry cross vault, successfully capturing the collapse mechanisms.

Additional research focused on the influence of masonry as an orthotropic material on the seismic response of this type of structural element is needed to further validate the numerical approach. In addition, a validation of the DMEM considering the application of textile-reinforced mortar as a strengthening technique for this element is an ongoing investigation.

7. References

Alforno, M., Venuti, F., Monaco, A., and Calderini, C. 2022. "Seismic behaviour of cross vaults with different brick pattern." *Bulletin of Earthquake Engineering* no. 20 (8):3921-3939.

Allemang, R. J. 1982. A correlation coefficient for modal vector analysis. In Proceedings of 1st International Modal Analysis Conference.

Angelillo, M., Babilio, E., and Fortunato, A. 2013. "Singular stress fields for masonry-like vaults." *Continuum Mechanics and Thermodynamics* no. 25 (2):423-41.

Angjeliu, G., Cardani, G., and Coronelli, D. 2019. "A parametric model for ribbed masonry vaults." *Automation in Construction* no. 105. doi: https://doi.org/10.1016/j.autcon.2019.03.006.

Angjeliu, G., Coronelli, D., Cardani, G., and Boothby, T. 2020. "Structural assessment of iron tie rods based on numerical modelling and experimental observations in Milan Cathedral." *Engineering Structures* no. 206.

ASTM E519/E519M – 10. 2010. Standard Test method for Diagonal Tension (Shear) in Masonry Assemblages.

Bertolesi, E., Adam, J. M., Rinaudo, P., and Calderón, P. A. 2019. "Research and practice on masonry cross vaults – A review." *Engineering Structures* no. 180:67-88.

Bianchini, N., Calderini, C., Mendes, N., Candeias, P. X., and Lourenço, P. B. 2023a. "Blind Prediction Competition - Sera.ta - Seismic Response of Masonry Cross Vaults: Shaking table tests and numerical validations (Version 1)." doi: https://doi.org/10.5281/zenodo.7624666.

Bianchini, N., Calderini, C., Mendes, N., Candeias, P. X., and Lourenço, P. B. 2023b. "Postdiction Competition - Sera.ta - Seismic Response of Masonry Cross Vaults: Shaking table tests and numerical validations (Version 1).". doi: https://doi.org/10.5281/zenodo.7624791.

Bianchini, N., Mendes, N., Calderini, C., Candeias, P. X., Rossi, M., and Lourenço, P. B. 2022. "Seismic response of a small-scale masonry groin vault: Experimental investiga tion by performing quasi-static and shake table tests." *Bulletin of Earthquake Engineering* no. 20 (3):1739–65. doi: https://doi.org/10.1007/s10518-021-01280-0.

Bianchini, N., Mendes, N., Calderini, C., and Lourenço, P. B. 2023c. "Modelling of the dynamic response of a reduced scale dry joints groin vault." *Journal of Building Engineering* no. 66:105826. doi: https://doi.org/10.1016/j.jobe.2023.105826.

Block, P., Ciblac, T., and Ochsendorf, J. 2006. "Real-time limit analysis of vaulted masonry buildings." *Computers & Structures* no. 84 (29):1841-1852.

Block, P., and Ochsendorf, J. 2007. "Thrust network analysis: a new methodology for three dimensional equilibrium." *Journal of the International Association for shell and spatial structures* no. 48 (3):167-73.

BS EN 772-1. 2011. Methods of test for masonry units.

Caddemi, S., Caliò, I., Cannizzaro, F., and Pantò, B. 2017. "New frontiers on seismic modeling of masonry structures." *Frontiers in Built Environment* no. 3:39. doi: https://doi.org/10.3389/fbuil.2017.00039.

Caliò, I., Marletta, M., and Pantò, B. 2012. "A new discrete element model for the evaluation of the seismic behaviour of unreinforced masonry buildings." *Engineering Structures* no. 40:237-338.

Caliò, I., and Pantò, B. 2014. "A macro-element modelling approach of Infilled Frame Structures." *Computers & Structures* no. 143:91-107.

Cannizzaro, F., Pantò, B., Caddemi, S., and Caliò, I. 2018. "A Discrete Macro-Element Method (DMEM) for the nonlinear structural assessment of masonry arches." *Engineering Structures* no. 168:243-256.

Cannizzaro, F., Pantò, B., Caddemi, S., and Caliò, I. 2023. "Discrete modelling of externally bonded composite layers on masonry structures." *Composite Structures* no. 315:116937. doi: https://doi.org/10.1016/j.compstruct.2023.116937.

Casolo, S., and Peña, F. 2007. "Rigid element model for in-plane dynamics of masonry walls considering hysteretic behaviour and damage." *Earthquake Engineering & Structural Dynamics* no. 36:1029-1048.

Chiozzi, A., Milani, G., and Tralli, A. 2017. "Fast kinematic limit analysis of FRP-reinforced masonry vaults. I : General genetic algorithm – NURBS – based formulation." *Journal of Engineering Mechanics* no. 149 (9).

Coccia, S., and Como, M. 2015. "Minimum thrust of rounded cross vaults." *International Journal of Architectural Heritage* no. 9 (4):468–84.

Creazza, G., Matteazzi, R., Saetta, A., and Vitaliani, R. 2002. "Analyses of masonry vaults: a macro approach based on three-dimensional damage model." *Journal of Structural Engineering* no. 128 (5):646-654.

D'Asdia, P., and Viskovic, A. 1995. "Analyses of a masonry wall subjected to horizontal actions on its plane, employing a non-linear procedure using changing shape finite elements." *Transactions on Modelling and Computer Simulation* no. 10:519-26.

De Lorenzis, L., Dimitri, R., and La Tegola, A. 2007. "Reduction of the lateral thrust of masonry arches and vaults with FRP composites." *Construction and Building Materials* no. 21 (7):1415–30.

De Matteis, G., and Mazzolani, F. M. 2010. "The Fossanova Church: seismic vulnerability assessment by numeric and physical testing." *International Journal of Architectural Heritage* no. 4 (3):222-45.

EN 1015-11. 2006. Methods of Test for Mortar for Masonry - Part 11: Determination of flexural and compressive strength of hardened mortar.

EN 1052-1. 1998. Methods of test for masonry - Part 1: determination of compressive strength.

EN 1052-3. 2002. Methods of test for masonry - Part 3: determination of initial shear strength

Fagone, M., Rotunno, T., and Bati, S. B. 2016. "The groin vaults of St. John Hospital in Jerusalem: an experimental analysis on a scale model." *International Journal of Architectural Heritage* no. 10 (7):903-918. doi: https://doi.org/10.1080/15583058.2016.1158331.

Foraboschi, P. 2004. "Strengthening of masonry arches with fiber-reinforced polymer strips strengthening of masonry arches with fiber-reinforced polymer strips." *Journal of Composites for Construction* no. 8 (3):191:202.

Foti, D., Vacca, V., and Facchini, I. 2018. "DEM modeling and experimental analysis of the static behavior of a dry-joints masonry cross vaults." *Construction and Building Materials* no. 170:111–20.

Fraternali, F. 2010. "A thrust network approach to the equilibrium problem of unreinforced masonry vaults via polyhedral stress functions." *Mechanics Research Communications* no. 37 (2):198–204.

Gaetani, A., Bianchini, N., and Lourenço, P. B. 2021. "Simplified micro-modelling of masonry cross vaults: stereotomy and interface issues." *International Journal of Masonry Research and Innovation* no. 6 (1):97-125. doi: 10.1504/IJMRI.2021.112076.

Gaetani, A., Lourenço, P. B., Monti, G., and Milani, G. 2017. "A parametric investigation on the seismic capacity of masonry cross vaults." *Engineering Structures* no. 148:686-703.

Ghiassi, B., and Milani, G. 2019. *Numerical modeling of masonry and historical structures: from theory to application*: Woodhead Publishing.

Gruppo Sismica s.r.l. 2015. "HiStrA (Historical Structure Analysis)." *Release 17.2.3*.

Kappos, A. J., Penelis, G. G., and Drakopoulos, C. G. 2002. "Evaluation of Simplified Models for Lateral Load Analysis of Unreinforced Masonry Buildings." *Journal of Structural Engineering* no. 128 (7):890–897.

Krajewski, P., and Hojdys, Ł. 2014. "Experimental Studies on Buried Barrel Vaults." *International Journal of Architectural Heritage* no. 9 (7):834–843. doi: https://doi.org/10.1080/15583058.2013.860499.

Lengyel, G. 2017. "Discrete element analysis of gothic masonry vaults for self-weight and horizontal support displacement." *Engineering Structures* no. 148:195–209.

Lengyel, G., and Bagi, K. 2015. "Numerical analysis of the mechanical role of the ribs in groin vaults." *Computers & Structures* no. 158:42–60. doi: https://doi.org/10.1016/j.compstruc.2015.05.032.

Magenes, G., and Della Fontana, A. 1998. "Simplified non-linear seismic analysis of masonry buildings." *Proc British Masonry Society* no. 8:190-5.

Marques, R., and Lourenço, P. B. 2011. "Possibilities and comparison of structural component models for the seismic assessment of modern unreinforced masonry buildings." *Computers & Structures* no. 89:2079–91.

McInerney, J., and DeJong, M. J. 2014. "Discrete Element Modeling of Groin Vault Displacement Capacity." *International Journal of Architectural Heritage* no. 9 (8):1037–49.

Milani, E., Milani, G., and Tralli, A. 2008. "Limit analysis of masonry vaults by means of curved shell finite elements and homogenization." *International Journal of Solids and Structures* no. 45 (20):5258-88.

Milani, G. 2015. "Advances in Engineering Software Upper bound sequential linear programming mesh adaptation scheme for collapse analysis of masonry vaults." *Advances in Engineering Software* no. 79:91-110.

Milani, G., Milani, E., and Tralli, A. 2009. "Upper bound limit analysis model for FRP – reinforced masonry curved structures. Part II : Structural analyses." *Computers & Structures* no. 87 (23-24):1534–58.

Milani, G., Rossi, M., Calderini, C., and Lagomarsino, S. 2016. "Tilting plane tests on a small-scale masonry cross vault: Experimental results and numerical simulations through a heterogeneous approach." *Engineering Structures* no. 123:300-312. doi: https://doi.org/10.1016/j.engstruct.2016.05.017.

Milani, G., Simoni, M., and Tralli, A. 2014. "Advanced numerical models for the analysis of masonry cross vaults: a case-study in italy." *Engineering Structures* no. 76:339–58. doi: https://doi.org/10.1016/j.engstruct.2014.07.018.

Milani, G., and Tralli, A. 2012. "A simple meso-macro model based on SQP for the non-linear analysis of masonry double curvature structures." *International Journal of Solids and Structures* no. 49 (5):808–34.

Pantò, B., Cannizzaro, F., Caddemi, S., Caliò, I., Chácara, C., and Lourenço, P. B. 2017a. "Nonlinear Modelling of Curved Masonry Structures after Seismic Retrofit through FRP Reinforcing." *Buildings* no. 7:79. doi: 10.3390/buildings7030079.

Pantò, B., Cannizzaro, F., Caliò, I., and Lourenço, P. B. 2017b. "Numerical and experimental validation of a 3D macro-model for the in-plane and out-of-plane behaviour of unreinforced masonry walls." *International Journal of Architectural Heritage*. doi: 10.1080/15583058.2017.1325539.

Penna, A., Lagomarsino, S., and Galasco, A. 2014. "A nonlinear macroelement model for the seismic analysis of masonry buildings." *Earthquake Engineering & Structural Dynamics* no. 43 (2):159-179. doi: 10.1002/eqe.2335.

Rossi, M., Barentin, C. C., Van Mele, T., and Block, P. 2017. "Experimental study on the behaviour of masonry pavilion vaults on spreading supports." *Structures* no. 11:110-20. doi: https://doi.org/10.1016/j.istruc.2017.04.008.

Rossi, M., Calderini, C., and Lagomarsino, S. 2016. "Experimental testing of the seismic in-plane displacement capacity of masonry cross vaults through a scale model." *Bulletin of Earthquake Engineering* no. 14 (1):261-281. doi: https://doi.org/10.1007/s10518-015-9815-1.

Russell, D. M. 1997. Error measures for comparing transient data: part I: development of a comprehensive error measure. In Proceedings of Proceedings of the 68th shock and vibration symposium.

Saloustros, S., Pelà, L., and Roca, P. 2020. "Nonlinear Numerical Modeling of Complex Masonry Heritage Structures Considering History-Related Phenomena in Staged Construction Analysis and Material Uncertainty in Seismic Assessment." *Journal of Performance of Constructed Facilities* no. 34 (5). doi: https://doi.org/10.1061/(ASCE)CF.1943-5509.0001494.

Santini, S., Baggio, C., Sabbatini, V., and Sebastiani, C. 2022. "Seismic assessment of roman concrete groin vaults through UAV, NDT and 3D Analyses." *Heritage* no. 5 (1):311-313.

Scacco, J., Milani, G., and Lourenço, P. B. 2020. "Automatic mesh generator for the non-linear homogenized analysis of double curvature masonry structures." *Advances in Engineering Software* no. 150.

Structural Vibration Solution. 2015. "ARTeMIS SVS User's Manual (8.4)."

Takeda, T., Sozen, M. A., and Nielsen, N. N. 1970. "Reinforced concrete response to simulated earthquakes." *Journal of the Structural Division* no. 96 (12):2557-2573.

Theodossopoulos, D., and Sinha, B. 2008. Structural safety and failure modes in Gothic vaulting systems. In Proceedings of 8th International Seminar on Structural Masonry, at Instanbul.

Theodossopoulos, D., Sinha, B. P., A.S., U., and Macdonald, A. J. 2002. "Assessment of the structural response of masonry cross vaults." *Strain* no. 38:119-27.

Theodossopoulos, D., Sinha, B. P., and Usmani, A. S. 2003. "Case study of the failure of a cross vault: Church of Holyrood Abbey." *Journal of architectural engineering* no. 9 (3):109-17.

Torres, B., Bertolesi, E., Moragues, J. J., Calderón, P. A., and Adam, J. M. 2019. "Experimental investigation of a full-scale timbrel masonry cross vault subjected to vertical settlement." *Construction and Building Materials* no. 221:421-432.

Turnsek, V., and Cacovic, F. 1971. Some experimental result on the strength of brick masonry walls. In Proceedings of 2nd International Brick Masonry Conference, at Stoke-on-Trent, UK.

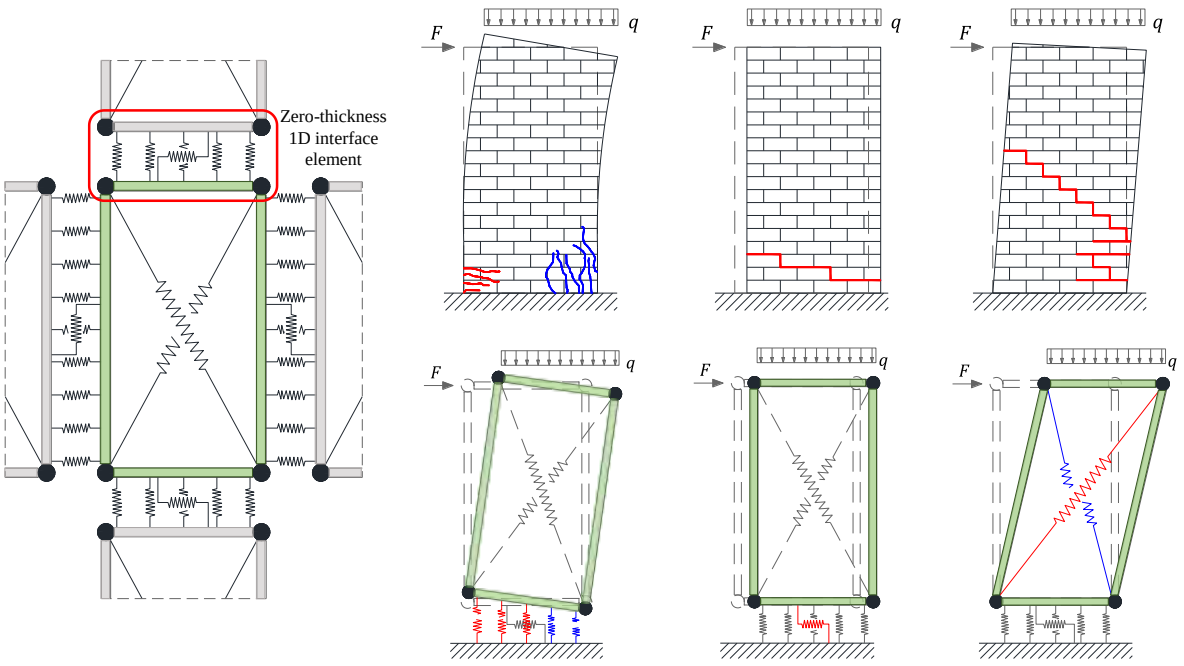

(a) (b) (c) (d)

Figure 1. Initial mechanical scheme of DMEM: (a) 2D panel and (b) flexural, (c) shear-sliding and (d) shear-diagonal in-plane mechanisms.

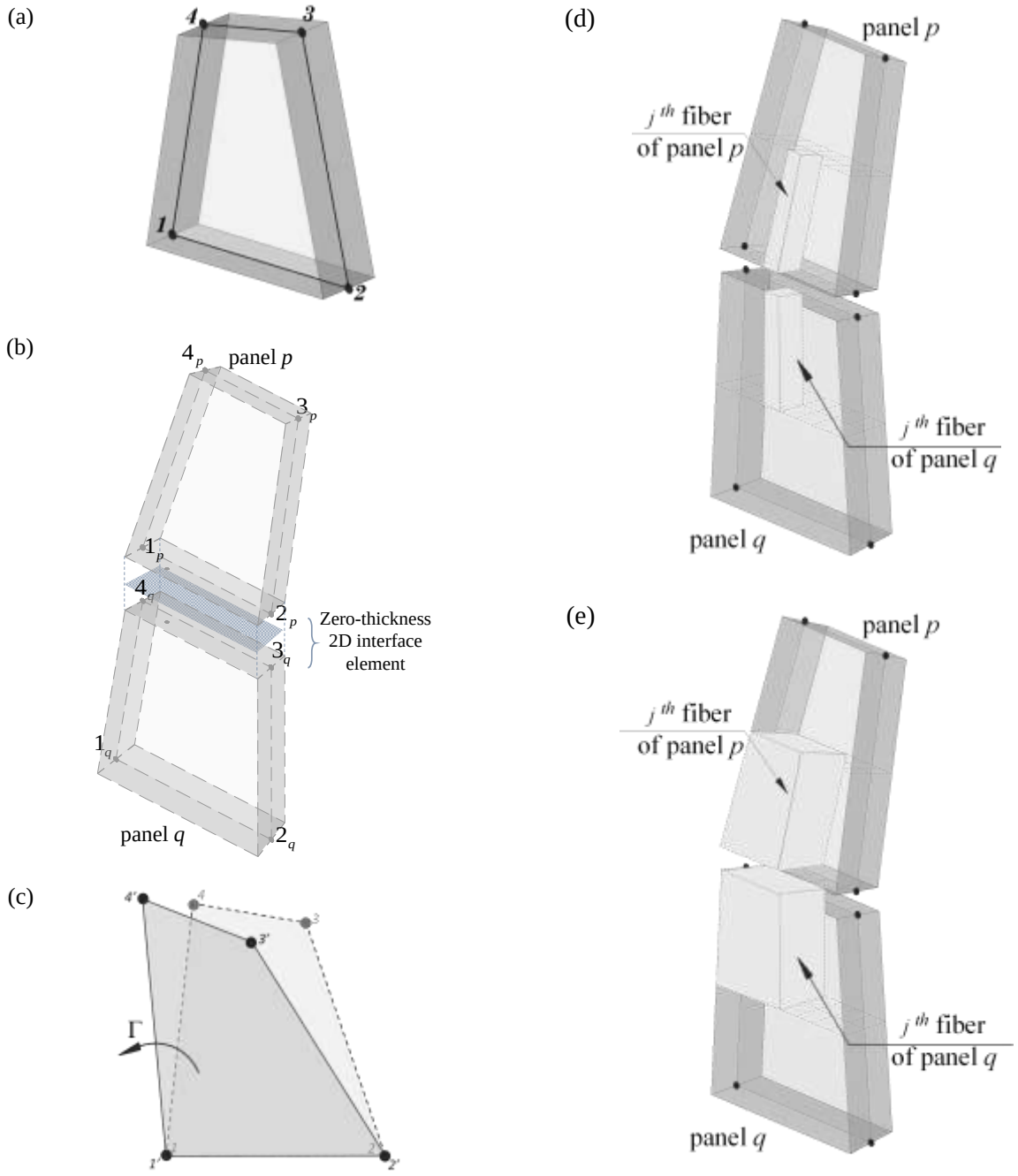

Figure 2. Upgraded mechanical scheme of DMEM: (a) 3D panel, (b) connection of panels by 2D interface element, (c) in-plane shear deformability, (d) fiber approach-based flexural calibration, and (e) fiber approach-based out-of-plane calibration.

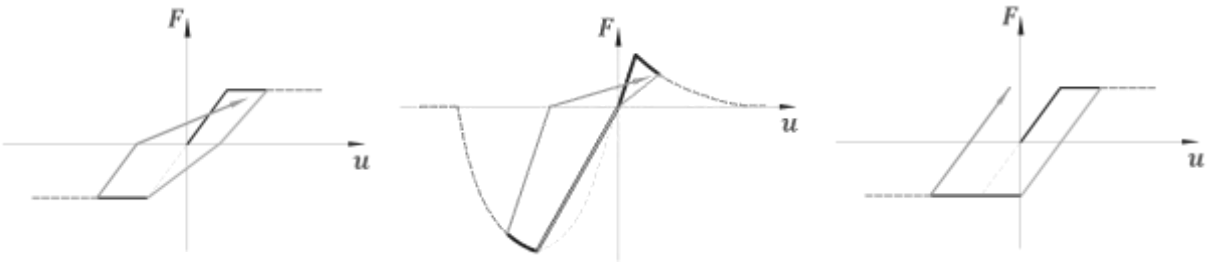

(a) (b) (c)

Figure 3. Constitutive and hysteretic models for: (a) diagonal, (b) transversal, and (c) sliding links.

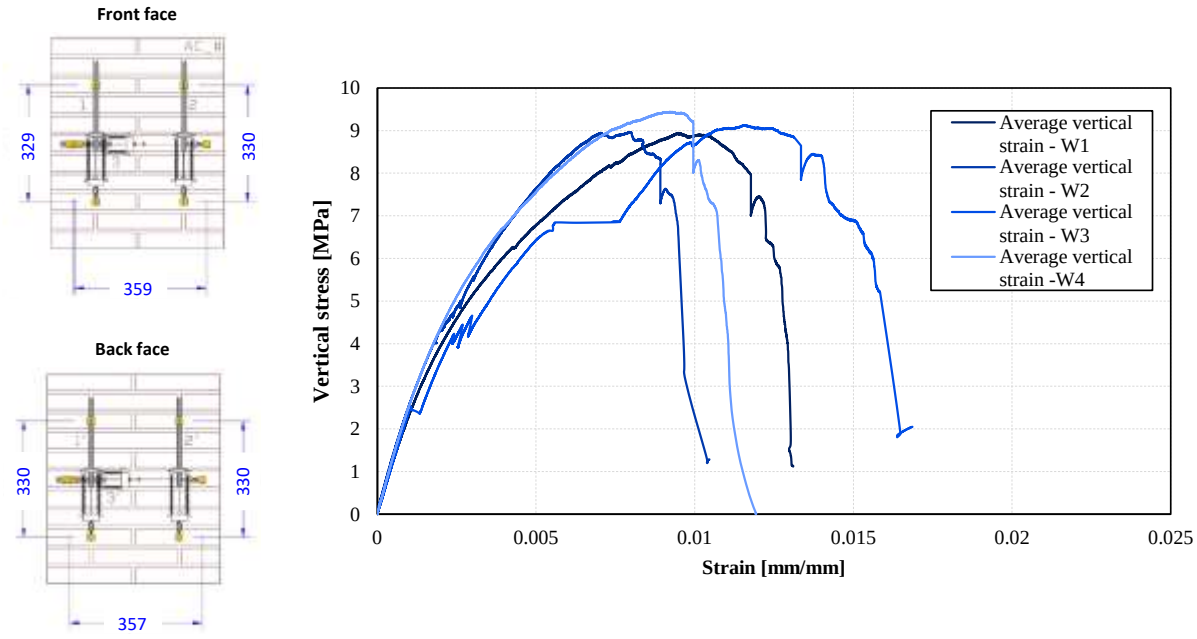

(a) (b)

Figure 4. Uniaxial compression tests on masonry wallets: (a) instrumentation setup and (b) stress-strain curves.

(adapted from (Bianchini et al., 2023a))

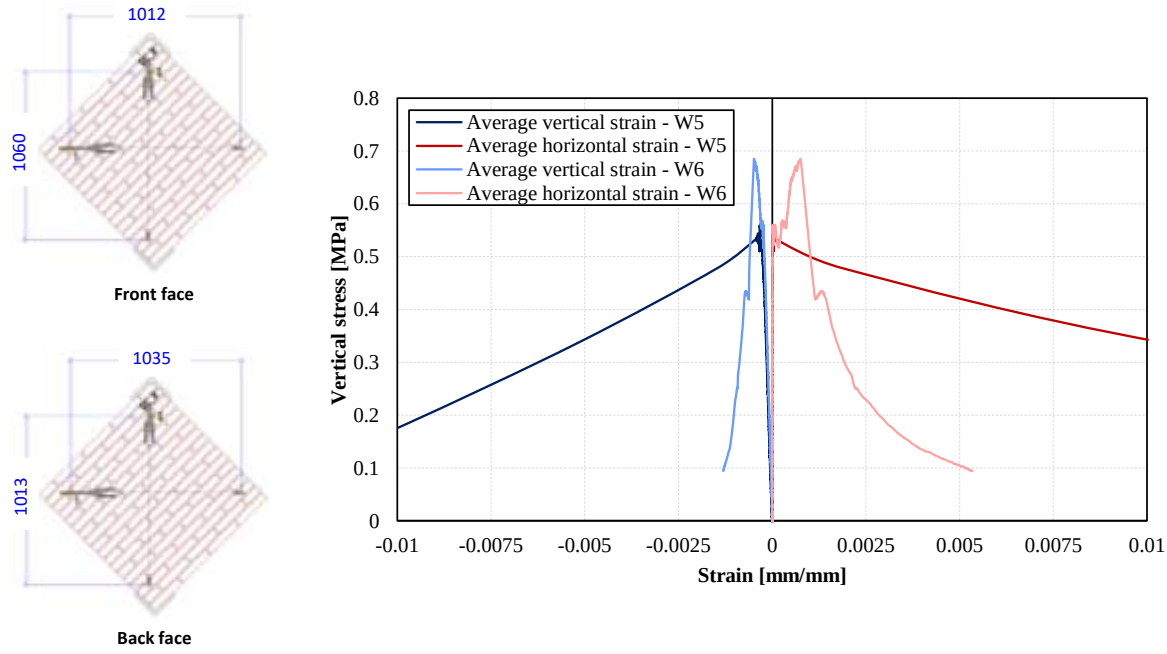

(a) (b)

Figure 5. Diagonal compression tests on masonry wallets: (a) instrumentation setup, and (b) stress-strain curves.

(adapted from (Bianchini et al., 2023a))

Figure 6. Experimental setup for the application of triplet shear tests to fired brick masonry specimens. (adapted from (Bianchini et al., 2023a))

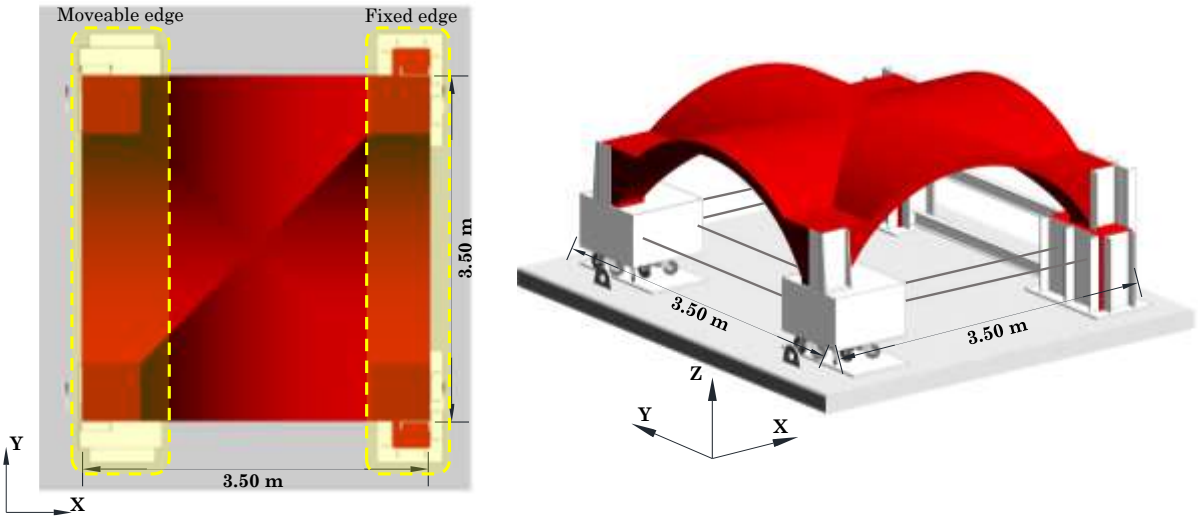

(a) (b)

Figure 7. Geometrical layout and boundary conditions of the unstrengthened masonry cross vault: (a) plan and (b) isometric views.

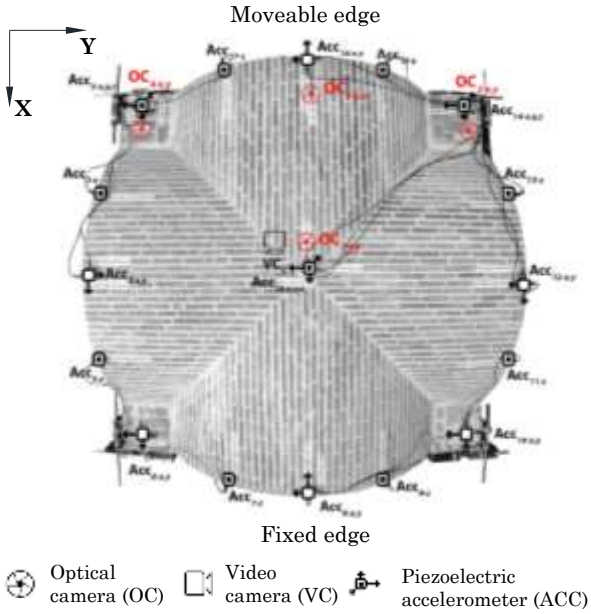

Figure 8. Instrumentation setup for the dynamic identification and shaking table tests (Bianchini et al., 2023a).

		1st mode	2nd mode	3rd mode
Mode shapes		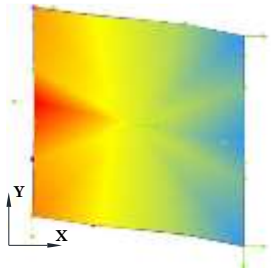	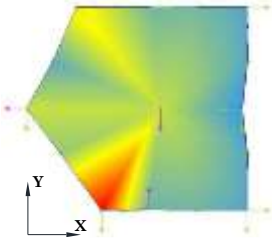	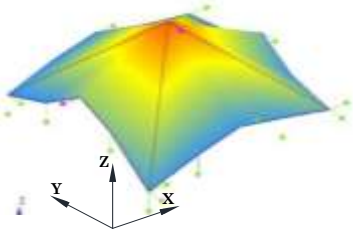
Frequency	DIT 0	6.15 Hz	11.62 Hz	19.39 Hz
	DIT 1	6.15 Hz	11.38 Hz	19.38 Hz
	DIT 2	5.89 Hz	10.79 Hz	19.30 Hz
	DIT 3	5.57 Hz	10.10 Hz	-

Figure 9. Mode shapes and natural frequencies of the unstrengthened masonry cross vault (Bianchini et al., 2023b).

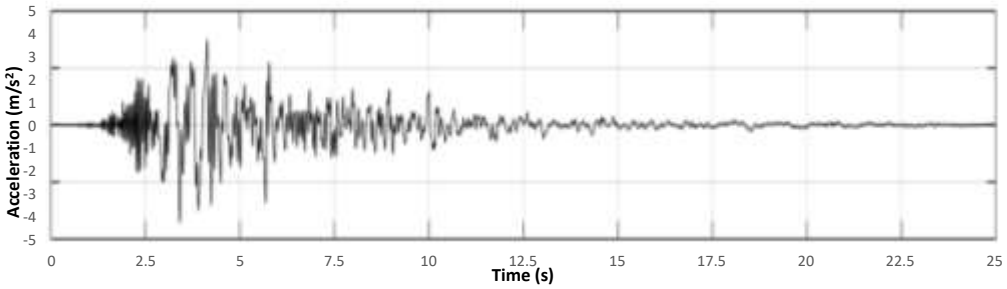

Figure 10. Filtered history of acceleration considered for the shaking table tests (Bianchini et al., 2023b).

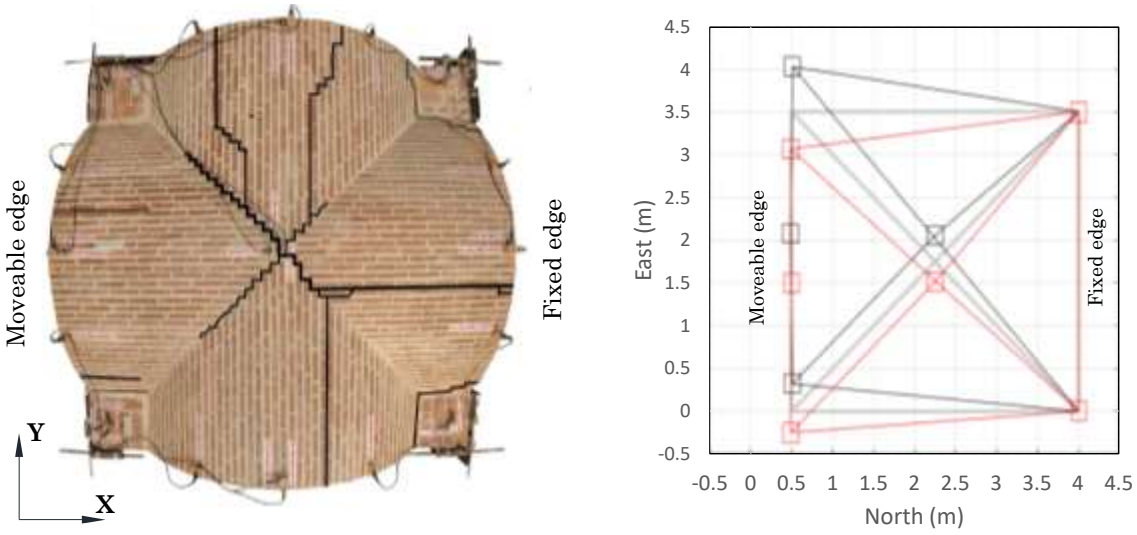

(a) (b)

Figure 11. Experimental response of unstrengthened masonry cross vault subjected to shaking table tests: (a) failure mechanism, and (b) maximum deformed configuration (Bianchini et al., 2023b).

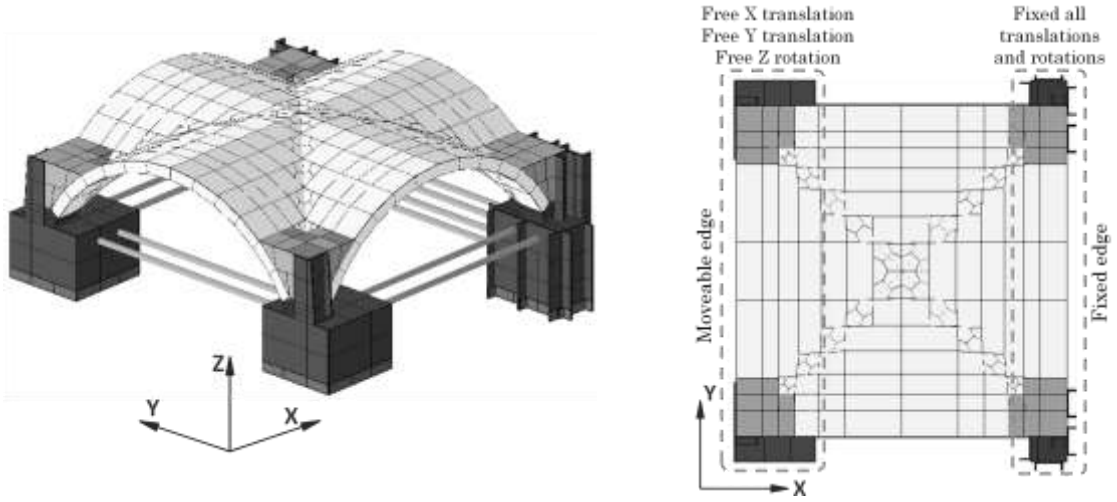

(a) (b)

Figure 12. DMEM numerical model: (a) 3D and (b) top-plan views

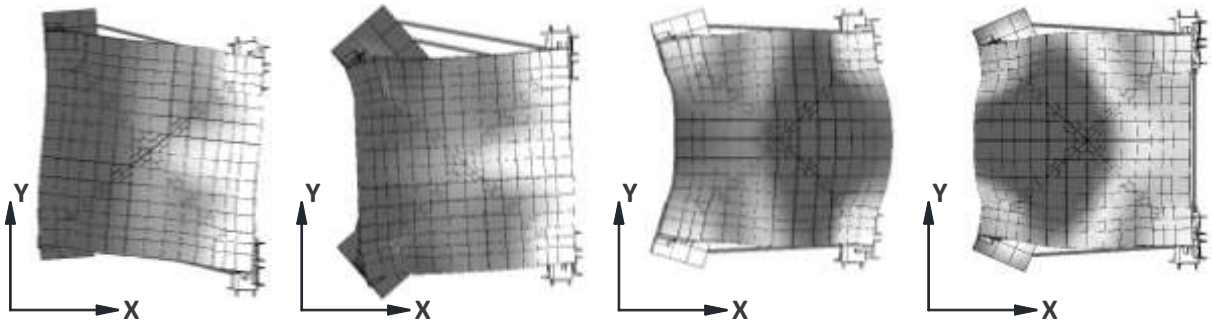

f_1 = 7.30 Hz f_2 = 20.63 Hz f_3 = 20.84 Hz f_4 = 23.64 Hz

Figure 13. Plan view of the first four vibration modes obtained with the DMEM model.

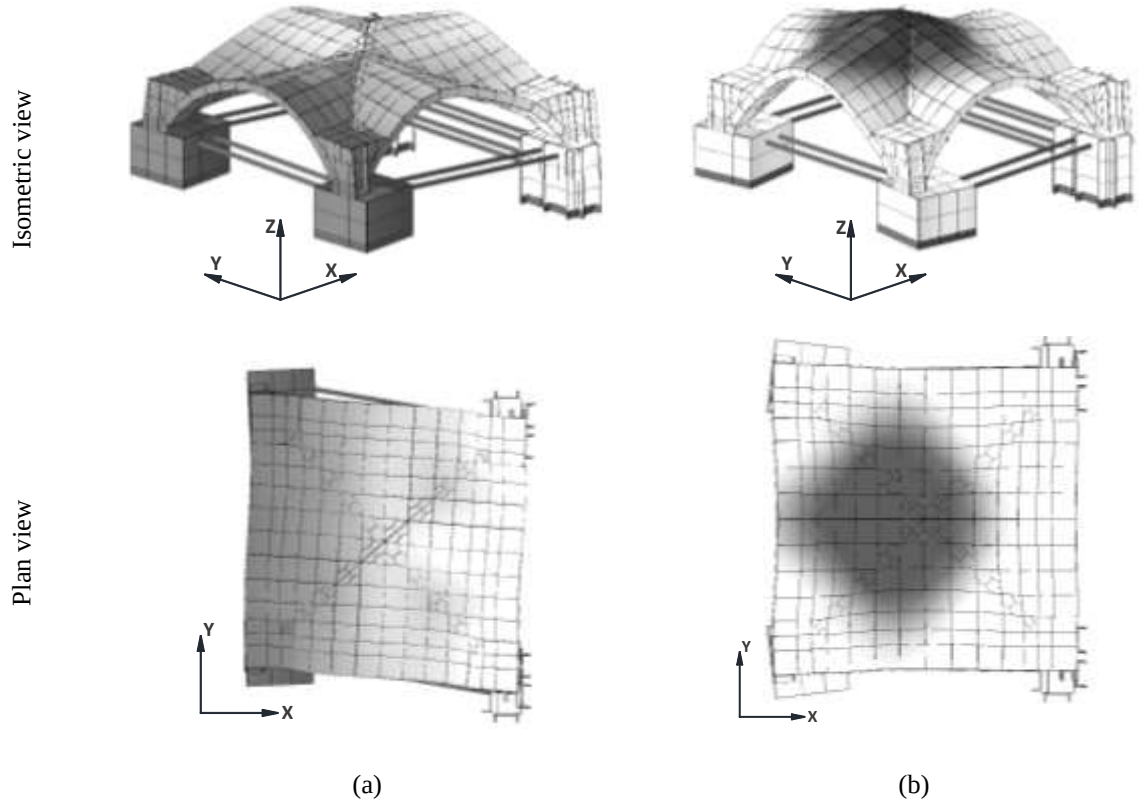

Figure 14. DME dynamic properties: (a) first and (b) fourth vibration modes

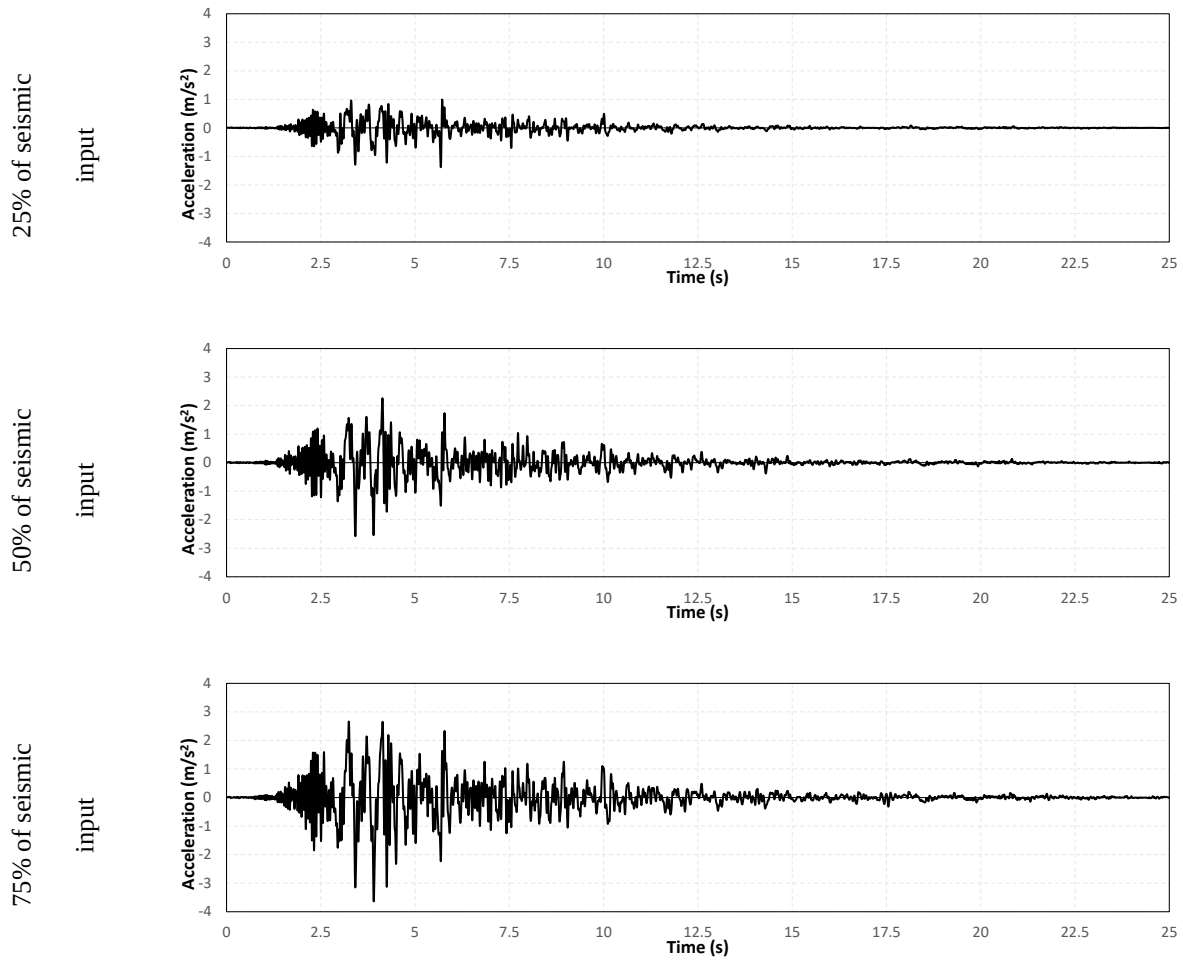

Figure 15. Histories of acceleration recorded at the base of the shaking table.

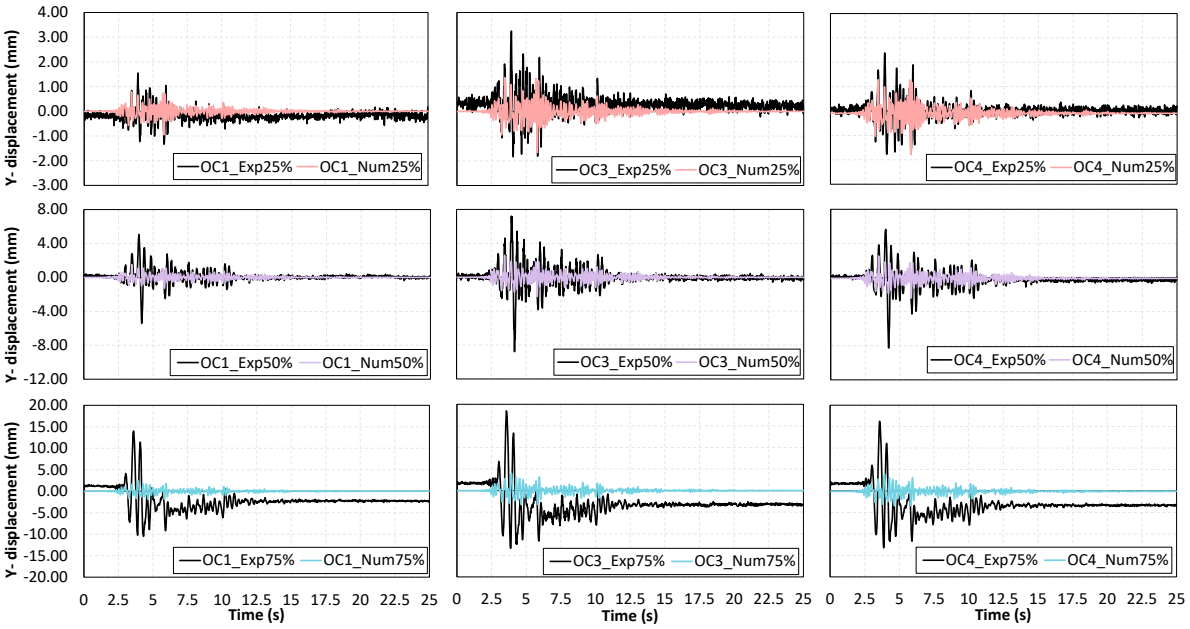

Figure 16. Comparison between experimental and numerical histories of displacement considering the nominal masonry nonlinear mechanical properties.

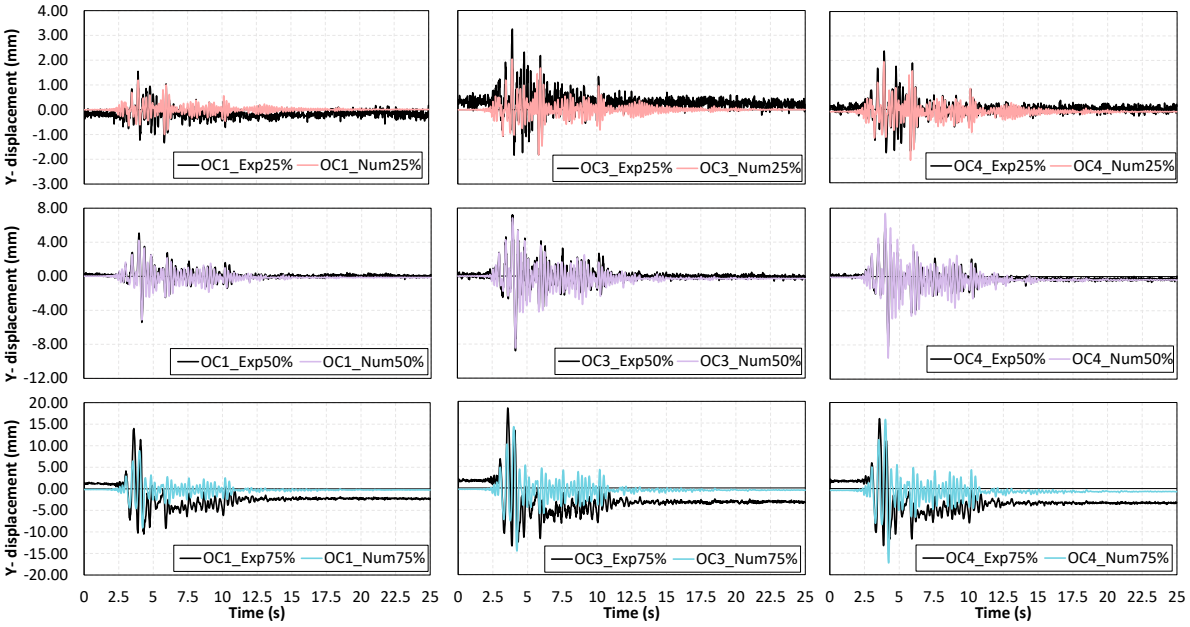

Figure 17. Comparison between experimental and numerical histories of displacement considering mechanical properties after sensitivity analysis.

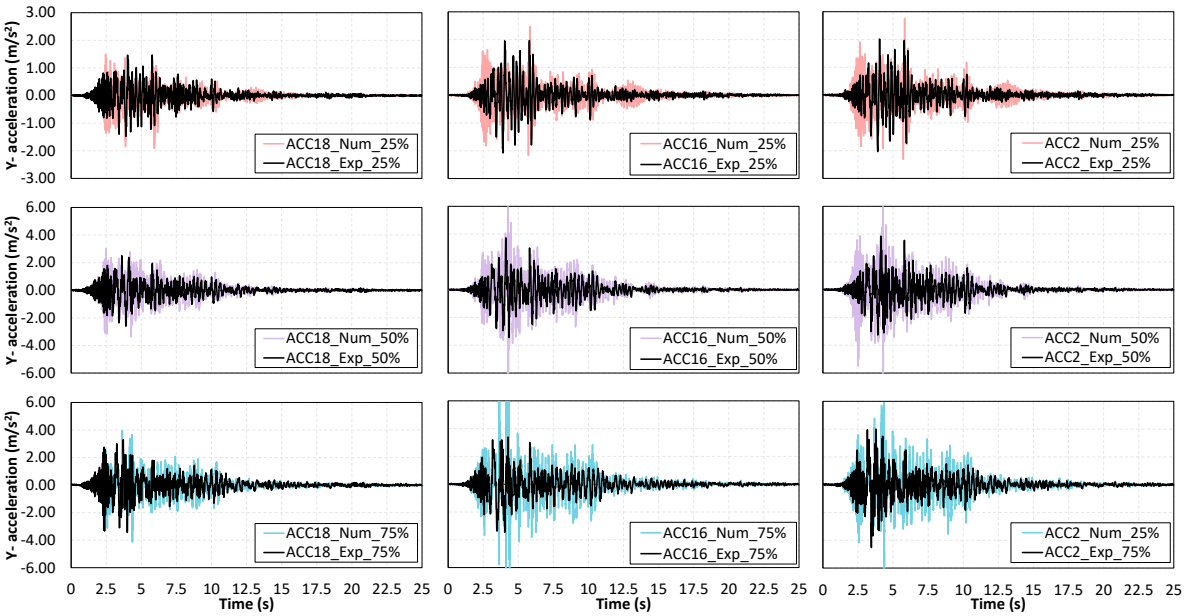

Figure 18. Comparison between experimental and numerical histories of acceleration considering mechanical properties after sensitivity analysis.

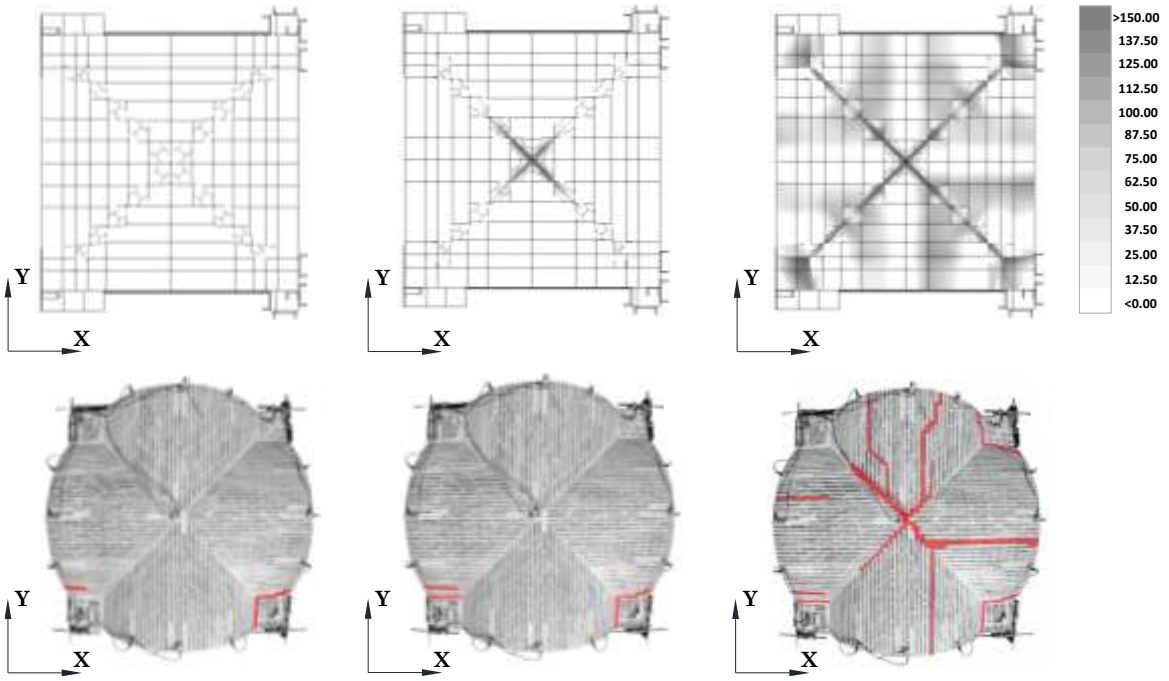

(a) (b) (c)

Figure 19. Plastic strains ratio of the DMEM model and experimental crack pattern after the application of: (a) 25%, (b) 50%, and (c) 75% of seismic intensity.

Table 1. Mechanical properties of solid fired brick units and cement mortar (Bianchini et al., 2023a).

		σ	COV
Solid fired brick units	Density	2204 kg/m^3	1.5%
	Young's modulus	6200 MPa	10.3%
	Compressive strength	25 MPa	3.3%
Hydraulic lime mortar	Density	1747 kg/m^3	0.7%
	Young's modulus	370 MPa	15.6%
	Compressive strength	1.68 MPa	10.1%
	Flexural strength	0.66 MPa	16.5%

Table 2. The sequence of dynamic identification and shaking table tests performed during the experimental campaign.

ID	Test	Description
DIT 0	Dynamic identification	Under no damage condition
STT 1	Shaking table	Considering 10% of seismic input 2009 L'Aquila
STT 2		Considering 25% of seismic input 2009 L'Aquila
DIT 1	Dynamic identification	After 25% of the seismic input
STT 3	Shaking table	Considering 50% of seismic input 2009 L'Aquila
DIT 2	Dynamic identification	After 50% of the seismic input
STT 4	Shaking table	Considering 75% of seismic input 2009 L'Aquila
DIT 3	Dynamic identification	After 75% of the seismic input

Table 3. Frequency and mode shape comparison between experimental and numerical results.

Modes		Initial	RF = 0.9	RF = 0.8	RF = 0.7	**RF = 0.6**	RF = 0.5
1st num vs 1st exp	f_{num} [Hz]	7.30	6.99	6.66	6.31	**5.92**	5.48
	abs error [%]	18.58	13.63	8.29	2.51	**3.83**	10.89
	MAC [-]	0.852	0.854	0.855	0.856	**0.865**	0.860
4th num vs 3rd exp	f_{num} [Hz]	23.64	21.98	21.02	19.94	**19.34**	18.70
	abs error [%]	21.96	17.88	13.39	8.42	**2.85**	3.55
	MAC [-]	0.473	0.530	0.597	0.667	**0.735**	0.791

Table 4. Nominal nonlinear mechanical properties of fired brick masonry

Nonlinear properties	Flexural	Compressive strength	f_c	MPa	9.10
		Compressive fracture energy	G_c	N/m	1456
		Tensile strength	f_t	MPa	0.44
		Tensile fracture energy	G_t	N/m	20.0
	Shear-sliding	Cohesion	c	MPa	0.66
		Friction coefficient	μ_s	-	0.79

Table 5. Comparison between experimental and numerical histories of displacement.

		25% of seismic input			50% of seismic input			75% of seismic input		
		OC1	OC3	OC4	OC1	OC3	OC4	OC1	OC3	OC4
Maximum displacement error	[%]	23	37	18	17	5	31	37	23	1
Minimum displacement error	[%]	25	1	17	5	4	15	14	9	30
Magnitude error ε_M	[-]	0.31	0.30	0.09	-0.01	-0.08	-0.17	0.47	0.38	0.32
Phase error ε_P	[-]	0.33	0.28	0.28	0.22	0.21	0.18	0.37	0.35	0.35